Coupling to two target-state bands in the study of the $n+^{22}$Ne system at low energy

P. R. Fraser,[1,2,3,*] L. Canton,[1] K. Amos,[2,4] S. Karataglidis,[2,4] J. P. Svenne,[5] and D. van der Knijff[2]

[1]*Istituto Nazionale di Fisica Nucleare, Sezione di Padova, Padova I-35131, Italy*
[2]*School of Physics, University of Melbourne, Victoria 3010, Australia*
[3]*Department of Imaging and Applied Physics, Curtin University, Bentley, Western Australia 6102, Australia*
[4]*Department of Physics, University of Johannesburg, P.O. Box 524 Auckland Park, 2006, South Africa*
[5]*Department of Physics and Astronomy, University of Manitoba, and Winnipeg Institute for Theoretical Physics, Winnipeg, Manitoba, Canada R3T 2N2*

One theoretical method for studying nuclear scattering and resonances is via the multichannel algebraic scattering (MCAS) formalism. Studies to date with this method have used a simple collective-rotor prescription to model target states with which a nucleon couples. While generally these target states all belong to the same rotational band, for certain systems it is necessary to include coupling to states outside of that main band. Here, we extend MCAS to allow coupling of different strengths between such states and the rotor band. This is an essential consideration in studying the example examined herein, the scattering of neutrons from ^{22}Ne.

I. INTRODUCTION

As an example of the effects of considering states that weakly couple to those within a collective band, we examine neutron scattering from ^{22}Ne. Besides the study of the mass-23 isobars being of interest inherently, the formation of these nuclei by radiative capture is of great astrophysical interest [1,2]. For example, it is important to understand the processes leading to their presence in white dwarf stars, as ^{23}Ne and ^{23}Na form an Urca pair [3], emitting neutrinos and delaying a supernova explosion. Such type Ia supernovae have properties which are thought usable to measure the extent and expansion of the universe.

Another topical problem associated with these isobars is the so-called ^{22}Na puzzle of ONe white dwarf novae [4–6], where the abundance of ^{22}Na predicted by existing stellar models is not found, indicating there is yet more to learn about how the distribution of elements in the universe occurred. Two reactions possibly pertinent to this loss of abundance are ^{22}Mg$(p,\gamma)^{23}$Al and ^{22}Na$(p,\gamma)^{23}$Mg. MCAS is well suited to modeling the ^{22}Mg$(p,p)^{22}$Mg reaction (the mirror is the system studied here) due to the low density of low-energy states in ^{23}Al and the low scattering threshold. This is a necessary first step in analyzing the resonant capture ^{22}Mg$(p,\gamma)^{23}$Al using the formalism of Ref. [7]. Development of the MCAS project to obtain capture cross-section values is in progress.

This study is also a prelude to that of the $p+^{22}$Ne system, since that scattering and the associated capture cross section is important in astrophysics. It is part of the hydrogen-burning NeNa cycle which may occur in second-generation stars. Speculated leakage from the CNO cycles into the NeNa cycle is linked to the problem of anticorrelations having been observed between sodium and oxygen when stars ascend the red giant branch of the Hertzsprung-Russell diagram, despite current stellar models predicting that the surface abundance of elements should not change. The rate of the ^{22}Ne$(p,\gamma)^{23}$Na reaction depends on the strengths of several resonances which have never been observed experimentally. Being afflicted by extremely large uncertainties [8], theoretical treatment of both resonant and direct capture will be desirable to complement experimental investigations performed at LUNA [9] at $E <$ 400 keV. Indeed, they are topics of future work.

The multichannel algebraic scattering (MCAS) formalism [10] is one with which scattering observables and spectra for quantum systems can be evaluated. To date it has been used for nuclear processes. In the MCAS method, solutions of coupled-channel Lippmann-Schwinger equations are found in momentum space using finite-rank expansions of an input matrix of nucleon-nucleus interactions. A set of Sturmian functions is used as the expansion basis. The MCAS method is able to locate all compound-system resonance centroids and widths, regardless of how narrow, and has the ability to determine subthreshold bound states by using negative energies. Further, use of orthogonalizing pseudopotentials (OPP) in generating Sturmians, ensures that the Pauli principle is not violated [11,12], even with a collective model formulation of nucleon-nucleus interactions. Otherwise, some compound nucleus wave functions possess spurious components [13].

Having the purview of low-energy scattering, with a range of a few MeV, MCAS usually deals with target nuclei in which only one mode of collective behavior is exhibited. To date, the Tamura [14] collective model with rotational character has been used to determine a coupled-channel interaction with nucleons. Thus, target states selected for coupling should be from within the principal rotation band of nuclei which exhibit such behavior, and the β_L (which determines the coupling strengths) is the same coupling amongst all states. Often, these calculations reproduce scattering observables very well, and even possess predictive power [11,15,16]. At times, however, it is necessary to include coupling to states outside of this band, for example where experiment has shown γ decays to states within a clearly defined collective band. Here, we extend MCAS to allow coupling of different strengths between such states and those in the rotor band.

*prfraser@unimelb.edu.au

Section II shows details of the development of MCAS rotor potentials for NA scattering, adding two facets to that previously published [10]: a generalization to allow more than one multipole deformation, and an extension to allow a second band for a given deformation. As $n+^{22}$Ne is the system selected to illustrate these developments. Section III shows results of a no-core $(0+2)\hbar\omega$ shell model calculation for ^{22}Ne, allowing insight into structure of orbit occupancy of the target states. Section IV shows a method of identifying the ratio of β_2 values linking second-band states to first-band states, examines the effect of having different β_2 bands on the calculated spectrum, and determines which channels are important in describing the $n+^{22}$Ne system. Results are shown for both spectra and elastic cross section. Finally, in Sec. VI, conclusions are drawn.

II. A TALE OF TWO β_Ls

To illustrate the manner in which different coupling strengths between channels stemming from different target states are considered, the development of the rotational-type coupled-channel NA-scattering potential is summarized. How these potentials are treated with the MCAS solution of the coupled-channel Lippmann-Schwinger equations is covered in detail in Ref. [10].

With channels defined by

$$c = [(l\tfrac{1}{2})jI; JM], \tag{1}$$

$(l\tfrac{1}{2})j$ are the orbital, intrinsic spin, and total angular momentum of relative motion of the projectile on the target, I is the total angular momentum of the target state involved, and J,M are the angular momentum quantum numbers of the compound system. Then, we define a NA coupled-channels potential matrix by

$$V_{cc'}(r) = f(r)\{V_0\delta_{cc'} + V_{ll}[\ell\cdot\ell]_{cc'} + V_{ss}[\mathbf{s}\cdot\mathbf{I}]_{cc'}\} + g(r)V_{ls}[\ell\cdot\mathbf{s}]_{cc'}, \tag{2}$$

in which local form factors have been assumed, and parameters of the potential governing central (V_0), orbit-orbit (V_{ll}), spin-spin (V_{ss}), and spin-orbit ($V_{\ell s}$) components. (Note that, being a parameter of the model, V_{ls} contains the constant $2\lambda_\pi^2$, where λ_π is related to the inverse of the pion Compton wave length.) We identify the functions $f(r)$ and $g(r)$ with deformed Woods-Saxon form factors:

$$f(r) = [1 + e^{(\frac{r-R}{a})}]^{-1}; \quad g(r) = \frac{1}{r}\frac{df(r)}{dr}. \tag{3}$$

To introduce a rotor character for this general nucleon-nucleus interaction potential, let us first consider that the quantum radius of a rigid drop of nuclear matter, with axial, permanent deformation from the spherical, is represented by the expansion

$$R(\theta,\phi) = R_0\left[1 + \sum_{L(\geqslant 2)}\sqrt{\frac{4\pi}{2L+1}}\beta_L\,[\mathbf{Y}_L(\hat{r})\cdot\mathbf{Y}_L(\hat{\Upsilon})]\right]$$

$$= R_0[1+\epsilon], \tag{4}$$

where $(\hat{r}) = (\theta,\phi)$ designates internal target coordinates. $\hat{\Upsilon}$ are Euler angles specifying the transformation from body-fixed to space-fixed frame co-ordinates.

Expanding $f(r)$ in Eq. (2) to second order in ϵ gives

$$f(r) = f_0(r) + \epsilon\left(\frac{\partial f(r)}{\partial\epsilon}\right)_0 + \frac{1}{2}\epsilon^2\left(\frac{\partial^2 f(r)}{\partial\epsilon^2}\right)_0. \tag{5}$$

We wish to convert these derivatives to being in terms of r. If we demand that $f(r) = f(r - R(\theta,\phi))$, that for every r there is an accompanying subtraction of R, we use the following:

$$\frac{\partial f(r)}{\partial\epsilon} = \frac{\partial f(r-R)}{\partial R}\frac{\partial R}{\partial\epsilon} = -R_0\frac{\partial f(r-R)}{\partial r}. \tag{6}$$

Thus,

$$f(r) = f_0(r) - R_0\sum_{L(\geqslant 2)}\sqrt{\frac{4\pi}{2L+1}}\beta_L\,[\mathbf{Y}_L(\hat{r})\cdot\mathbf{Y}_L(\hat{\Upsilon})]\frac{df_0(r)}{dr}$$

$$+ \frac{1}{2}R_0^2\left[\sum_{L(\geqslant 2)}\sqrt{\frac{4\pi}{2L+1}}\beta_L\,[\mathbf{Y}_L(\hat{r})\cdot\mathbf{Y}_L(\hat{\Upsilon})]\right]^2$$

$$\times\frac{d^2 f_0(r)}{dr^2}. \tag{7}$$

Keeping L general, and not assuming $L = L'$, i.e., that only one β of deformation is considered, we obtain

$$\epsilon^2 = \left[\sum_{L(\geqslant 2)}\sqrt{\frac{4\pi}{2L+1}}\beta_L\,[\mathbf{Y}_L(\hat{r})\cdot\mathbf{Y}_L(\hat{\Upsilon})]\right]^2$$

$$= \sum_{L,L'(\geqslant 2)}\frac{4\pi\beta_L\beta_{L'}}{\sqrt{(2L+1)(2L'+1)}}$$

$$\times[\mathbf{Y}_L(\hat{r})\cdot\mathbf{Y}_L(\hat{\Upsilon})]\,[\mathbf{Y}_{L'}(\hat{r})\cdot\mathbf{Y}_{L'}(\hat{\Upsilon})]. \tag{8}$$

Using a property of tensor products [17], we can express

$$[\mathbf{Y}_L(\hat{r})\cdot\mathbf{Y}_L(\hat{\Upsilon})]\,[\mathbf{Y}_{L'}(\hat{r})\cdot\mathbf{Y}_{L'}(\hat{\Upsilon})]$$

$$= \frac{(2L+1)(2L'+1)}{4\pi}$$

$$\times\sum_\ell\frac{1}{2\ell+1}|\langle L0L'0|\ell 0\rangle|^2\,[\mathbf{Y}_\ell(\hat{r})\cdot\mathbf{Y}_\ell(\hat{\Upsilon})], \tag{9}$$

where ℓ runs from $|L - L'|$ to $L + L'$, with the condition that $L + \ell + L'$ is even. Thus,

$$f(r) = f_0(r) - R_0\sum_{L(\geqslant 2)}\sqrt{\frac{4\pi}{2L+1}}\beta_L\,[\mathbf{Y}_L(\hat{r})\cdot\mathbf{Y}_L(\hat{\Upsilon})]\frac{df_0(r)}{dr}$$

$$+ \frac{1}{2}R_0^2\sum_{L,L'(\geqslant 2)}\beta_L\beta_{L'}\sqrt{(2L+1)(2L'+1)}$$

$$\times\sum_\ell\frac{1}{2\ell+1}|\langle L0L'0|\ell 0\rangle|^2\,[\mathbf{Y}_\ell\cdot\mathbf{Y}_\ell]\frac{d^2 f_0(r)}{dr^2}. \tag{10}$$

A similar equation applies for the expansion of $g(r)$ in terms of the deformation ϵ.

As the full potential is now rather detailed, we consider it in terms of its zeroth, first and second order expansion

components:

$$
\begin{aligned}
V_{cc'}(r) &= V_{cc'}^{(0)}(r) + V_{cc'}^{(1)}(r) + V_{cc'}^{(2)}(r) \\
&= \{v^{(0)}(r)\}_{cc'} \\
&\quad + \left\{ v^{(1)}(r) \sum_{L(\geqslant 2)} \beta_L \sqrt{\frac{4\pi}{2L+1}} \; [\mathbf{Y}_L \cdot \mathbf{Y}_L] \right\}_{cc'} \\
&\quad + \left\{ v^{(2)}(r) \sum_{L,L'(\geqslant 2)} \beta_L \beta_{L'} \sqrt{(2L+1)(2L'+1)} \right. \\
&\quad \left. \times \sum_{\ell} \frac{1}{2\ell+1} |\langle L0L'0|\ell 0\rangle|^2 \; [\mathbf{Y}_\ell \cdot \mathbf{Y}_\ell] \right\}_{cc'} . \quad (11)
\end{aligned}
$$

This is a short-hand notation; as we focus on the β_L, the functions $v^{(0)}(r)$, $v^{(1)}(r)$ and $v^{(2)}(r)$ are employed to subsume all terms independent of L, concerning the derivatives of the Woods-Saxon form factors and potential variables. For completeness, these are shown in full in the Appendix, where the interplay of spin-angular operators and multipole deformations are taken into account.

The above development is similar to that of Ref. [10], but is generalised to consider more than one multipole deformation; that is, cases where $L \neq L'$. (N.B. This development has been used previously [16], but heretofore has not been presented in detail.)

Next, we consider cases where there exist states which are outside the main rotational band, but which are known to couple to states in the rotor band. To describe this weaker coupling, it is necessary to include, for a given L, an additional value of β_L, which we denote here as $\overline{\beta_L}$. This can be done with a scaling, viz.

$$
\overline{\beta_L} = s_L \beta_L , \quad (12)
$$

whereby Eq. (11) becomes

$$
\begin{aligned}
V_{cc'}(r) &= \{v^{(0)}(r)\}_{cc'} \\
&\quad + \left\{ v^{(1)}(r) \sum_{L(\geqslant 2)} s_L \beta_L \sqrt{\frac{4\pi}{2L+1}} \; [\mathbf{Y}_L \cdot \mathbf{Y}_L] \right\}_{cc'} \\
&\quad + \left\{ v^{(2)}(r) \sum_{L,L'(\geqslant 2)} s_L \beta_L s_{L'} \beta_{L'} \sqrt{(2L+1)(2L'+1)} \right. \\
&\quad \left. \times \sum_{\ell} \frac{1}{2\ell+1} |\langle L0L'0|\ell 0\rangle|^2 \; [\mathbf{Y}_\ell \cdot \mathbf{Y}_\ell] \right\}_{cc'} , \quad (13)
\end{aligned}
$$

where

$$
\begin{cases}
s_L = 1 & \text{if} \quad I_i^\pi\big|_c \;\text{ and }\; I_j^\pi\big|_{c'} \in \text{ main band} \\
0 < |s_L| < 1 & \text{if} \quad I_i^\pi\big|_c \;\text{ and/or }\; I_j^\pi\big|_{c'} \notin \text{ main band,}
\end{cases}
$$

I_i^π being the ith I^π target state, following the convention of the channel definition in Eq. (2). These changes of band correspond to a shape transition. In future works we intend to refine this coupling scheme such that it takes into account

differences between reorientation within a given band and transitions between different bands.

III. A SHELL MODEL FOR STATES IN ^{22}Ne

Before considering scattering of neutrons from ^{22}Ne as an example of the expansion of MCAS considered here, it is instructive to consider what can be gleaned about that target nucleus from shell-model studies of adequate complexity as has been used in Refs. [18–20].

We first sought results from a no-core $(0+2)\hbar\omega$ shell-model for ^{22}Ne. The OXBASH program [21] with the WBT interactions [22] was used. The single nucleon space chosen encompassed the 15 orbits in shells from the $1s_{\frac{1}{2}}$ through the $1g_{\frac{9}{2}}$-$3s_{\frac{1}{2}}$, Those evaluations involved such large dimensioned matrices that only vectors and energy values of the positive parity $J \leqslant 2$ states in the low-energy excitation spectrum of ^{22}Ne could be found. Allowing all 22 nucleons to be active is beyond the capacity of the standard OXBASH program we have used to find higher spin states and, as the associated vectors are very large, we have been unable as yet to extract many properties of those states. The results given then are preliminary to a planned fuller study which will include more nuclei in the mass region and made using a larger shell model program.

We have also made calculations within a reduced $(0\hbar\omega)$ space, the $1d$-$2s$ shell for ^{22}Ne, to give some indication of the major shell transition strengths between the 2_1^+ and 2_2^+ and the ground states as those three are of special interest in the MCAS studies.

First consider the (preliminary) results found using the large-space shell model. The evaluated excitation energies for the low-lying 0^+ and 2^+ states are in good agreement with data, as is evident in the listing in Table I.

Also shown in the table are the percentage admixture of $0\hbar\omega$ and $2\hbar\omega$ components in each state description. All states are considerably mixed with, characteristically, 33% of $2\hbar\omega$ component.

Further, all states are specified by numerous partitions of the nucleons within the orbits. Those contributing the largest percentages (greater than 5%) are listed in Table II. These dominant partitions have the $1s$-$1p$ shells completely full

TABLE I. The low lying 0^+ and 2^+ state energy levels in ^{22}Ne compared with values determined using the large space shell model calculation described in the text. Energies are in MeV and component types are in percent.

State	Exp.	Shell model	$0\hbar\omega$	$2\hbar\omega$
$0_{g.s.}^+$	0.000	0.000	67.62	32.38
2_1^+	1.275	1.336	67.48	32.51
2_2^+	3.358	4.244	67.15	32.85
2_3^+	4.456	4.507	66.89	33.11
2_4^+	5.363	5.579	66.57	33.43
2_5^+	6.120	6.185	67.00	33.00
0_2^+	6.234	5.803	66.72	33.28
0_3^+		6.428	66.39	33.61

TABLE II. Dominant partition (total nucleons) percentages (values $\geqslant 5\%$) in the shell model ground, 0_2^+, 2_1^+, and 2_2^+ states of ^{22}Ne.

$1d_{\frac{5}{2}}$	$1d_{\frac{3}{2}}$	$2s_{\frac{1}{2}}$	$0_{\text{g.s.}}^+$ Percent	0_2^+ (5.803) Percent	2_1^+ (1.336) Percent	2_2^+ (4.244) Percent
4	2	0	7.82			
4	1	1		5.59	7.84	8.45
5	1	0	5.64		4.57	7.11
3	1	2		9.21		
5	0	1	6.67	8.13	15.65	12.08
4	0	2	12.47	21.59	6.43	6.88
6	0	0	20.05	5.00	14.16	14.12

(occupancies 4, 8, and 4) and those for the remaining six nucleons (two protons and four neutrons) are listed according to the shell indicated.

This shell model gave another 11 partitions for these states all having percentages of between 1 and 5%; four having a reduced occupancy in the $1p$ orbits (offset by some in the $2p$ orbits) and two more with occupancy in the $2d$ orbit. The $1d$-$2s$ shell is the most important in this description of these states, with components are spread over all three orbits of that shell, but the $\sim$33% involving the other shells is needed to find the best result for the spectrum. There are also numerous other entries having smaller ($<1\%$) amplitudes.

Including $2\hbar\omega$ components in shell model descriptions of nuclear states of several light-mass nuclei has lead to predictions of transition rates enhanced on those found limiting the structure evaluations to $0\hbar\omega$. Often the latter models require a significant polarization charge to give a match to measured $B(E2)$ rates and electron scattering form factors, for example, while some studies using larger space structures do not [18,19]. Nevertheless we next present results obtained using a $0\hbar\omega$ model (only the $1d$-$2s$ shell active with the USD interaction of Brown and Wildenthal [23]) to illustrate that the 2_1^+ and 2_2^+ states should both have non-negligible transition strength to the ground, though coupling to the 2_1^+ is dominant. The one body density matrices that link the 2_1^+ and the 2_2^+ states to the ground are given in Table III.

TABLE III. The shell model one-body-density matrix values in the $2s$-$1d$ shell linking the 2_1^+ and 2_2^+ states to the ground.

j_1	j_2	2_1^+ (1.366)	2_2^+ (4.244)
$1d_{\frac{5}{2}}$	$1d_{\frac{5}{2}}$	-0.9582	-0.1153
$1d_{\frac{5}{2}}$	$1d_{\frac{3}{2}}$	-0.3261	0.1030
$1d_{\frac{5}{2}}$	$2s_{\frac{1}{2}}$	-0.5945	-0.1140
$1d_{\frac{3}{2}}$	$1d_{\frac{5}{2}}$	0.3341	0.0503
$1d_{\frac{3}{2}}$	$1d_{\frac{3}{2}}$	-0.0886	-0.1142
$1d_{\frac{3}{2}}$	$2s_{\frac{1}{2}}$	0.2472	0.1433
$2s_{\frac{1}{2}}$	$1d_{\frac{5}{2}}$	-0.6954	-0.0830
$2s_{\frac{1}{2}}$	$1d_{\frac{3}{2}}$	-0.2073	0.0118

These quantities are defined by the (doubly reduced) matrices for $\Delta T = 0$, namely

$$S_{j_1 j_2 I=2} = \langle 0_{\text{g.s.}}^+ |||[a_{j_2}^\dagger \otimes \tilde{a}_{j_1}]^{(I=2)}||| 2_{(1,2)}^+ \rangle. \qquad (14)$$

It is clear that, from these shell model results, ground state coupling favors the 2_1^+ state, but there is some non-negligible strength to the 2_2^+ state; of between 10 and 30 % for most terms.

IV. INITIAL MCAS EVALUATION OF THE n + ^{22}Ne SYSTEM

The low-lying spectrum of ^{22}Ne consists of ground state of $J^\pi = 0^+$, a 2^+ state at 1.274 MeV, and a 4^+ state at 3.357 MeV. Directly above this comes a 2^+ state at 4.456 MeV which decays by $E2$ transition to the ground state [24].

The 0^+, 2^+, and 4^+ states, along with a state at 6.31 MeV designated $(6)^+$ in the literature [24], we characterize as a rotor behavior. The actual spectrum of ^{22}Ne to 7 MeV excitation is shown in Fig. 1. The rotor-like spacing of the principal band (shown in thick, solid lines) is evident.
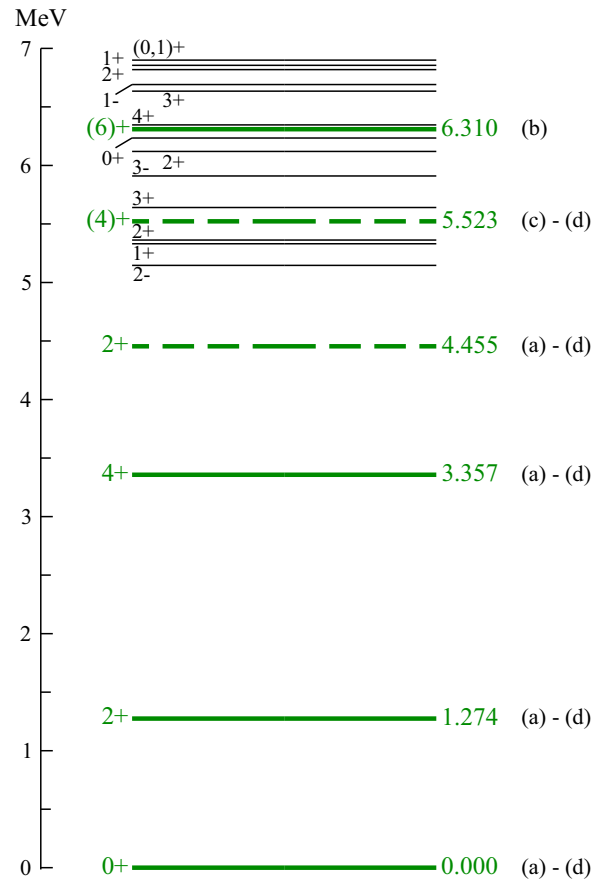

FIG. 1. (Color online) The low-energy experimental ^{22}Ne spectrum [24]. Thick, solid lines denote states of the ground-state band, thick dashed lines denote the other states used in this paper. Letters correspond to usage in specific calculations in Figs. 2, 5, and 6.

A. β_2 values for the two 2^+ states in ^{22}Ne.

Given that the 2_2^+ state (shown as a dashed line in Fig. 1) decays to the ground state but is not within the sequence of the first rotation-like band, we can expect that it exhibits some other degree of rotor character. Thus, we assign a different β_2 value (denoted $\overline{\beta_2}$ to distinguish it from that used for the main band) to link this state with those taken to be the principal rotor band.

The half-lives of states (ground state γ decay) relate to the transition probabilities (for $E2$ multipolarity) via

$$\tau_{\frac{1}{2}} = \frac{\ln(2)}{\mathcal{W}_{(E2)}(E_\gamma)} = \frac{0.693}{\mathcal{W}_{(E2)}(E_\gamma)} \quad (15)$$

and transition probabilities link to $B(E2)$ values via

$$\mathcal{W}_{(E2)}(E_\gamma) = 1.23 \times 10^9 \, (E_\gamma)^5 \, B(E2), \quad (16)$$

where E_γ is the photon energy.

To first order, and without consideration of band quantum numbers, a collective (rotational) model gives $B(E2)$ that are proportional to β_2^2.

For ^{22}Ne, the two low excitation 2^+ states (at 1.275 and 4.456 MeV) both decay by γ emission via $E2$ transitions to the ground state with half-lives of 3.63 ps and by 37 fs, respectively. Thus the relevant transition probabilities are

$$\mathcal{W}_{(E2)}(1.275) = \frac{0.693}{3.63} 10^{12}$$
$$= 1.23 \, 10^9 \, (1.275)^5 \, B(E2, 1.275),$$
$$\mathcal{W}_{(E2)}(4.456) = \frac{0.693}{37} 10^{15}$$
$$= 1.23 \, 10^9 \, (4.456)^5 \, B(E2, 4.456), \quad (17)$$

from which $B(E2, 1.275) = 46.06$ and $B(E2, 4.456) = 8.67$ (units are e^2 fm) and their ratio is 0.188. Then assuming that the $B(E2)$ scale as β_2^2, the deformation length for the 4.456 MeV decay would be ~0.43 times that for the 1.275 MeV decay, i.e., $\overline{\beta_2} = 0.43\beta_2$.

B. Results using the lowest four target states

For a scattering nucleon impinging upon a partially filled shell of a target nucleus, the Pauli principle does not necessarily imply a binary rule—that the shell is completely open or completely blocked [25–31]. We label as Pauli hindrance the intermediate situation, where the present nucleons do not completely, but only partially block additional nucleons. Considering such an interpretation, the dominant configurations of the shell model descriptions of the states in ^{22}Ne, shown in Table II, that are of particular interest in MCAS calculations prescribe full blocking of the $1s\frac{1}{2}$, $1p\frac{3}{2}$, and $1p\frac{1}{2}$ orbits, while suggesting Pauli hindrance for the $1d\frac{5}{2}, 1d\frac{3}{2}, 2s\frac{1}{2}$ orbits, meaning an orthogonalizing pseudopotential (OPP) that creates only a partial blocking of those d-s orbits. Those shell model functions further suggest that all higher subshells have essentially no blocking.

For simplicity, however, in this study we have considered purely allowed or purely blocked states. Consequently, parameters used to scale these OPP, denoted as $\lambda^{(OPP)}$ and in units

TABLE IV. Parameter values defining the $n+^{22}$Ne interaction. $\lambda^{(OPP)}$ are blocking strengths of occupied shells, in MeV.

	Odd parity	Even parity		
V_0 (MeV)	–65.20	–51.30		
V_{ll} (MeV)	–1.01	–0.30		
V_{ls} (MeV)	7.00	7.00		
V_{ss} (MeV)	–0.20	–1.45		
R_0	a	β_2	$\overline{\beta_2}$[a]	β_4
3.1 fm	0.75 fm	0.22	0.1034	–0.08
	$1s_{1/2}$	$1p_{3/2}$	$1p_{1/2}$	$1d_{5/2}$
0_1^+ $\lambda^{(OPP)}$	10^6	10^6	10^6	0.0
2_1^+ $\lambda^{(OPP)}$	10^6	10^6	10^6	0.0
4_1^+ $\lambda^{(OPP)}$	10^6	10^6	10^6	0.0
2_2^+ $\lambda^{(OPP)}$	10^6	10^6	10^6	0.0

[a]$\overline{\beta_2}$ for linking 2_2^+ to other states; 43% of 0.22. See Sec. IV A.

of MeV, are assigned a value of 10^6 MeV (which is adequate to remove all influence of blocked states) for the orbitals $1s\frac{1}{2}$, $1p\frac{3}{2}$, and $1p\frac{1}{2}$, and 0 MeV for $1d\frac{5}{2}$, as shown in Table IV. Full details of the Pauli principle in MCAS, including the blocking strengths of the OPP method, are given in Refs. [11,12].

The parameter set used to define the scattering potential is shown in Table IV. As with Ref. [32], which studied analyzing powers from ^{22}Ne$(p, p)^{22}$Ne, it was found that a small β_4 deformation of ^{22}Ne was required in MCAS. However, the best-fit MCAS deformations differ from those of Ref. [32] (being $\beta_2 = 0.47$ and $\beta_4 = 0.05$), which is understandable given the differences between the models, where the MCAS potential includes V_0, V_{ll}, V_{ls}, and V_{ss} terms and the same radius and diffusivity for V_{ls} as the other terms, Ref. [32] uses V_0 and V_{ls} alone (with a different prescription for the latter), but with different radius and diffusivity for V_0 and V_{ls}. Despite this, both values are of the same order of magnitude in each paper. We note, however, that a value of $\beta_2 = 0.562$ was proposed in Ref. [33], based upon an adopted value of the reduced $B(E2)\uparrow$ from the 0^+ ground state to the 2^+ first excited state. While two values of β_2 are used in this work as $E2$ transitions are observed between rotor and non-rotor-like states in ^{22}Ne, the same value of β_4 is used in all instances throughout the paper. In Ref. [4], studies of the mirror system ^{22}Mg$(p, p)^{22}$Mg were made using Glauber-type calculations [34]. In these, a Woods-Saxon potential was used (as it is in MCAS for nuclear and Coulomb potentials) for the proton binding potential, with standard nucleus radius (similar to ours) and diffuseness $a = 0.60$ fm.

The resultant MCAS spectrum of ^{23}Ne, relative to the scattering threshold, is shown in Fig. 2 for the energy range from the ground state to the scattering threshold. A number of states in the low-lying experimental spectrum are still not assigned with certainty [35]. With four of the fourteen states below -1 MeV having had more than one possible J^π suggested, and a further two between -1.5 and -1 MeV with no conjectured J^π, this MCAS evaluation makes an excellent match to the well-assigned states and can make a prediction of two of the four uncertainly assigned states. Specifically, the MCAS calculation suggests that the state at -3.5 MeV
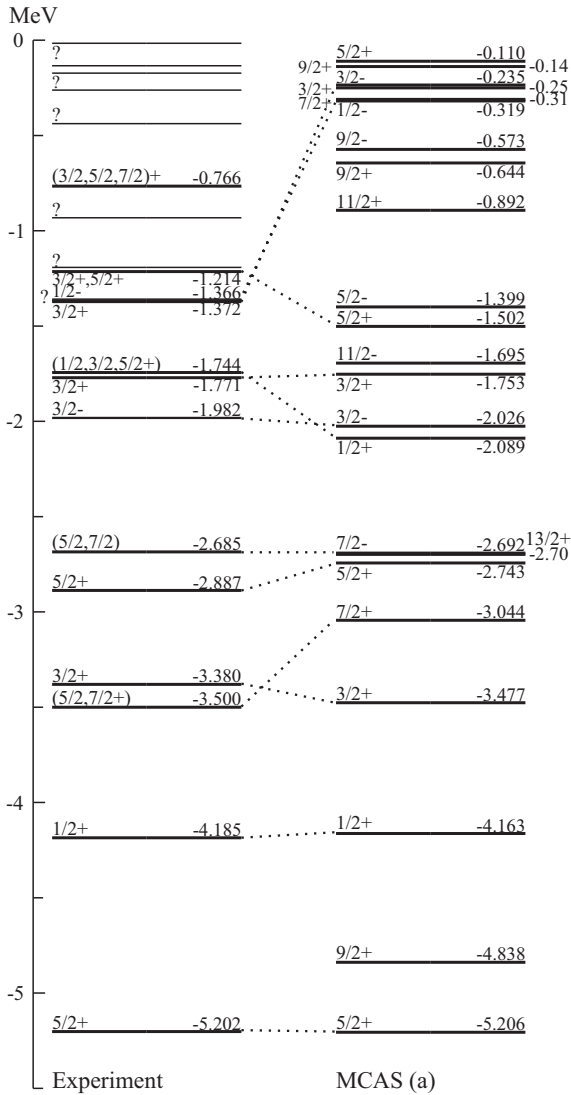
MeV

Experiment		MCAS (a)	
?		5/2+	−0.110
?		9/2+ 3/2−	−0.235 −0.14
		3/2+ 7/2+	−0.25
?		1/2−	−0.319 −0.31
		9/2−	−0.573
(3/2,5/2,7/2)+	−0.766	9/2+	−0.644
?		11/2+	−0.892
?			
?			
3/2+,5/2+	−1.214	5/2−	−1.399
? 1/2−	−1.366	5/2+	−1.502
3/2+	−1.372		
(1/2,3/2,5/2+)	−1.744	11/2−	−1.695
3/2+	−1.771	3/2+	−1.753
3/2−	−1.982	3/2−	−2.026
		1/2+	−2.089
(5/2,7/2)	−2.685	7/2−	−2.692 13/2+ −2.70
5/2+	−2.887	5/2+	−2.743
		7/2+	−3.044
3/2+	−3.380		
(5/2,7/2+)	−3.500	3/2+	−3.477
1/2+	−4.185	1/2+	−4.163
		9/2+	−4.838
5/2+	−5.202	5/2+	−5.206

FIG. 2. The experimental ^{23}Ne spectrum [35] and that calculated from MCAS evaluation of the $n+^{22}$Ne, with target state set (a): 0_1^+, 2_1^+, 4_1^+, $\overline{2_2^+}$. The bar denotes the use of reduced coupling for channels involving this state.

until now denoted $(\frac{5}{2},\frac{7}{2}^+)$ is a $\frac{7}{2}^+$, and the $(\frac{5}{2},\frac{7}{2})$ at −2.685 is a $\frac{7}{2}^-$. For the remaining uncertainly assigned states, MCAS gave states with the suggested spin-parities with energies in the proximity. We make no attempt to suggest spin-parities for states where none has been made previously, but we do note that the density of states above −1.5 MeV, where the number of states begins to tend towards continuum is recreated well by MCAS.

Regarding the $\frac{9}{2}^+$ state found by MCAS but not seen in experiment, it is possible that such state exists somewhere in this regime and is as yet unobserved. This is suggested by the existence of low-lying $\frac{9}{2}^+$ states in other mass-23 isobars. ^{23}Na, whose low-energy spectrum has many similarities with that of ^{23}Ne, has a $\frac{9}{2}^+$ state 2.703 MeV above the ground state, and its mirror, ^{23}Mg, has a state currently designated

$\frac{9}{2}^+$, $\frac{5}{2}^+$ at 2.714 MeV above the ground state. Preliminary development of extensions upon this work indicate that the $\frac{13}{2}^-$ at −2.696 MeV could be moved to higher energy by employing Pauli hindrance.

C. The effect of varying β_L values in MCAS

In Sec. IV A we illustrated an example of where it is advantageous to extend the MCAS formalism to allow pairs of coupling target states to have unique values of a given β_L. In that section, one method of selecting the ratio of these values was outlined. Herein, we perform a *gedanken* investigation where this scaling factor spans all values from 0 to 1.

The results of diverse MCAS calculations of the spectrum of ^{23}Ne to over 20 MeV excitation are given in Figs. 3 and 4. In Fig. 3, both the subthreshold and resonance parts of the spectrum are presented, while the subthreshold region is shown in greater detail in Fig. 4. The first MCAS calculation, the results of which are shown in the left most panels of these figures identified as '3-state', used just the three rotor-like states of ^{22}Ne (0_1^+, 2_1^+ and 4_1^+) finding in all 63 states (bound and resonant) as the spectrum of ^{23}Ne (with Pauli blocking included). The spectrum labeled '4-state, one β' in these figures resulted on using additionally the 2_2^+ state of ^{22}Ne with $\overline{\beta_2} = \beta_2$, giving a four-state MCAS calculation. The spectrum that results has 89 states of ^{23}Ne in the excitation energy range shown. The central panels show the results of four-state MCAS calculations allowing $\overline{\beta_2}$ to vary according to the scale variable $0 \leqslant s_2 \leqslant 1$ on β_2. The number of states for both the three-state and four-state calculations are shown, by J^π, in Table V.

Figure 4 shows the MCAS results for the subthreshold spectrum of ^{23}Ne. The spin-parities of the eleven most bound from the four-state evaluations are given. The effect of changing the scale factor, s_2, is most noticeable, with some states moving by as much as 2 MeV so that energy spacing and level sequence alters. The dashed line (at $s_2 = 0.43$) indicates the spectrum found when the ratios of $B(E2)$ values from the ground state γ decays of the 2_1^+ and 2_2^+ states define the scaling.

There are differences between the three-state result and the result of the four-state one when $s_2 = 0$. The disconnections are the result of two factors. The first is that while going from right to left in the central panels, the scaling of the β_2 is reduced from 1 to 0 but the scaling of $\beta_4 = -0.08$ is not, producing a small difference generated by the residual β_4 coupling. The remaining discontinuity comes from the spin-spin component of the zeroth-order term which links channels involving different target states having the same angular momentum, even with no deformation. This is evident in Eq. (A2) of the Appendix, wherein more details are given.

In the subthreshold region ($\lesssim -1$ MeV), the 3-state result has equivalent states with those of the four-state evaluations. That is not the case for higher energies, especially as shown in Fig. 3 in which the above threshold resonance centroids found from the same three- and four-state MCAS calculations are displayed. For energies $\geqslant -1$ MeV (see Fig. 4), the four-state model model gives 27 more states, most of which are resonances. The differences in resonance centroid energies
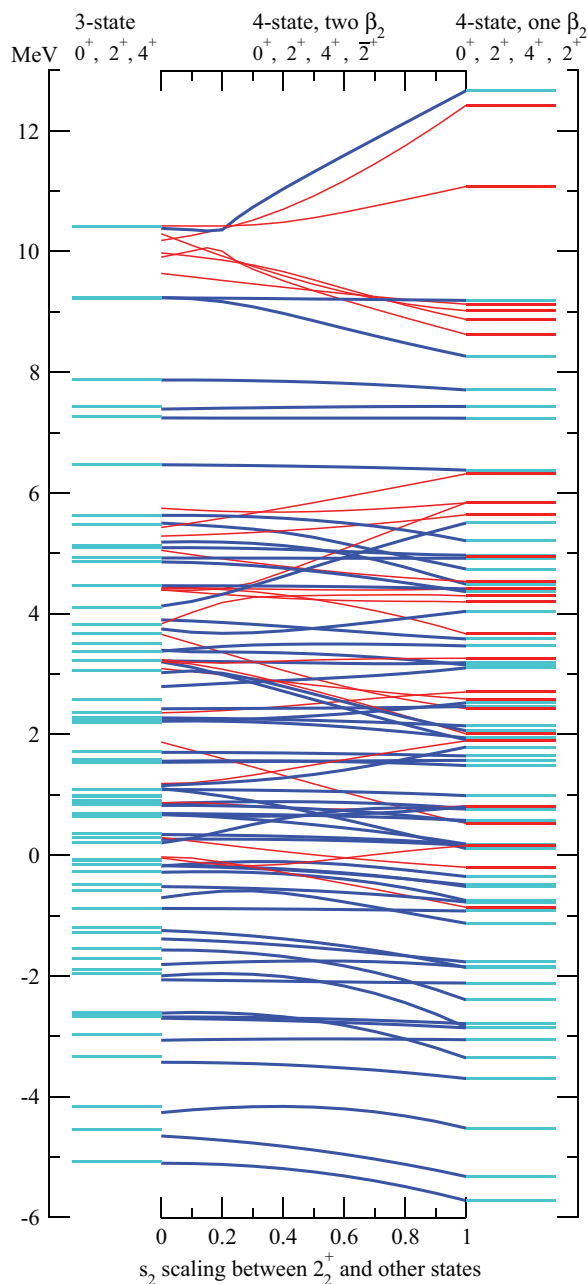
FIG. 3. (Color online) MCAS evaluation of $n+^{22}$Ne compound states with scaling of β_2 of ^{22}Ne 2_2^+ coupling. States shown by thin (red) lines are from coupling to the 2_2^+ state.
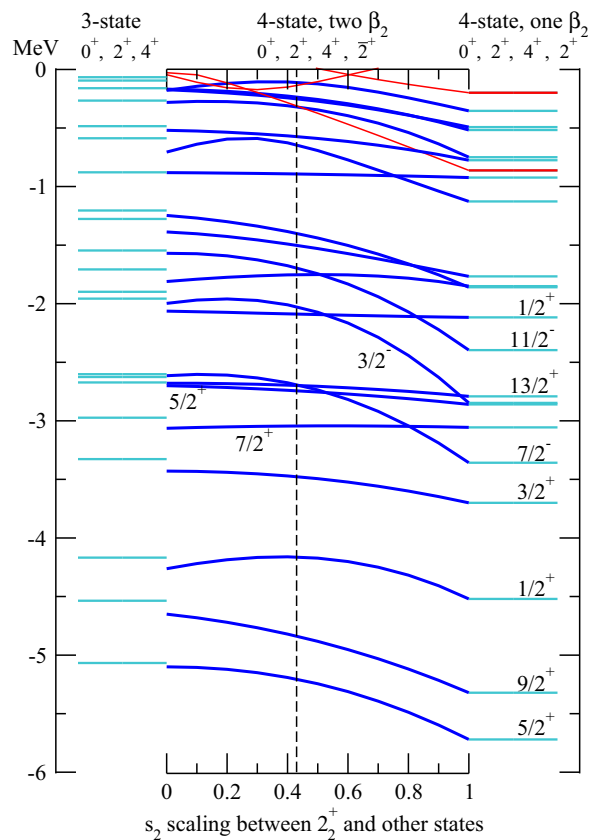

FIG. 4. (Color online) Detail of Fig. 3, showing subthreshold MCAS evaluation of the energy centroids of $n+^{22}$Ne resonances as β_2 of ^{22}Ne 2_2^+ coupling is scaled with respect to other couplings. The dashed line indicates value obtained from theory in Sec. IV A.

that the consideration of the ^{22}Ne 2_2^+ has a large impact on the ground and low-lying states of ^{23}Ne. Indeed, no ^{23}Ne spectrum from the resonances of $n+^{22}$Ne$_{0_1^+,2_1^+,4_1^+}$ achieved the level of agreement with data as that of the four-state calculation of Fig. 2. This is as would be expected, given that the 2_2^+ state is known to decay to the ^{22}Ne ground state.

V. THE EFFECTS OF ADDITIONAL CHANNELS

Given the result of Sec. IV C, it is instructive to examine the influence of additional channels on results.

A. Effects on the spectrum

The impact of including the next target state in the rotation-like band, that experimentally identified as $(6)^+$ at 6.310 MeV is now considered. This fits well with the typical rotational band spacing of the 0_1^+, 2_1^+, and 4_1^+ states. In

with variation of s_2 can be as much as 3 MeV and the sequencing of the states alters.

Thus, in addition to what is learnt in general about the effect of the varying the β_2 in an MCAS calculation, it is evident

TABLE V. Number of states by J^π. Pauli blocking reduces the numbers of states in each case.

J^π	$\frac{1}{2}^-$	$\frac{1}{2}^+$	$\frac{3}{2}^-$	$\frac{3}{2}^+$	$\frac{5}{2}^-$	$\frac{5}{2}^+$	$\frac{7}{2}^-$	$\frac{7}{2}^+$	$\frac{9}{2}^-$	$\frac{9}{2}^+$	$\frac{11}{2}^-$	$\frac{11}{2}^+$	$\frac{13}{2}^-$	$\frac{13}{2}^+$	$\frac{15}{2}^-$	Total
three-state	4	3	6	5	7	6	7	5	6	4	4	2	2	1	1	63
four-state	6	5	9	8	11	9	10	7	8	5	5	2	2	1	1	89
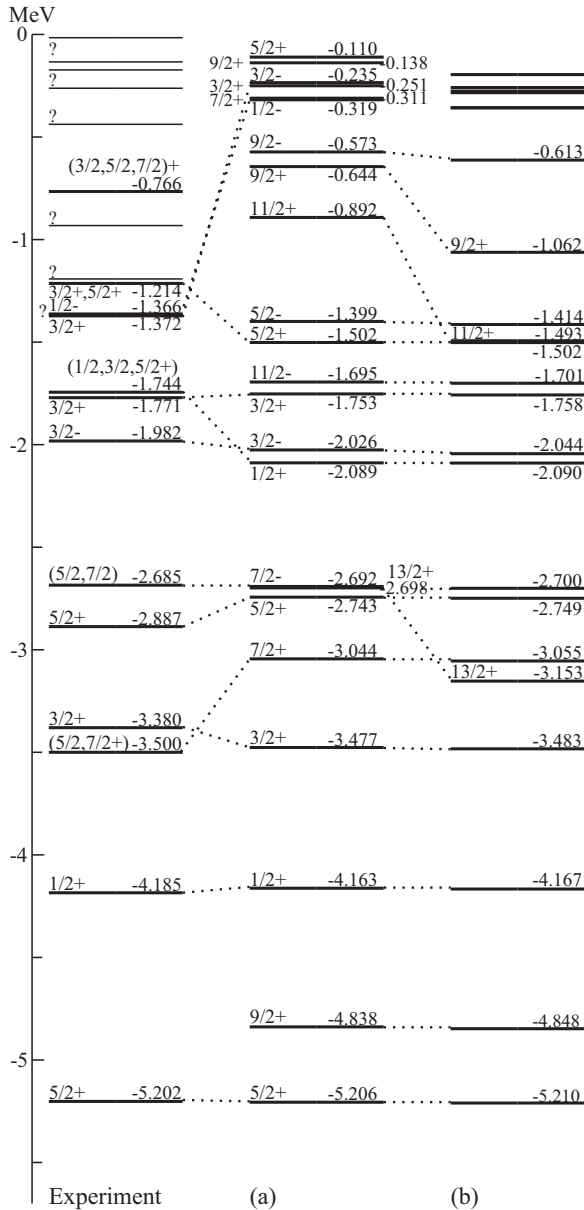
FIG. 5. Experimental data compared to MCAS ^{23}Ne spectra using (a) 0_1^+, 2_1^+, 4_1^+, $\overline{2_2^+}$ (as per Fig. 2); and (b) 0_1^+, 2_1^+, 4_1^+, $\overline{2_2^+}$, $(6)_1^+$. The bar in 2_2^+ denotes the use of reduced coupling for channels involving this state.

Fig. 5, the experimental spectrum of ^{23}Ne is compared with the MCAS calculation result of Fig. 2, denoted (a), and with that additionally including the 6^+ state, denoted (b). Both calculations use the parameter set of Table IV, which were tuned for (a), with the Pauli blocking strengths for the 6^+ state as per the others. Essentially the inclusion of this 6^+ state affects only the energies of the $\frac{9}{2}^+$, $\frac{11}{2}^+$, and $\frac{13}{2}^+$ states in this spectrum, adding to their binding.

Next we consider the influence of other states in the ^{22}Ne spectrum that may be weakly coupled to the ground state band. We include states deemed important in a study of the mirror system, $p+^{22}$Mg$\rightarrow^{23}$Al [4]. In Ref. [4], the configuration

mixing of the ground state of ^{23}Al was studied experimentally by observing the γ rays emitted by ^{22}Mg after proton emission. They found the relevant components to be ^{22}Mg$(0_1^+)\otimes p_{1d_{5/2}}$, with 18.5 of an observed 78.3 mb proton-emission cross section; ^{22}Mg$(2_1^+)\otimes p_{1d_{5/2}}$ and ^{22}Mg$(2_1^+)\otimes p_{2s_{1/2}}$ with 39.3 mb; ^{22}Mg$(4_1^+)\otimes p_{1d_{5/2}}$ with 9.5 mb; and ^{22}Mg$((4)_2^+)\otimes p_{1d_{5/2}}$ with 10.9 of 78.3 mb observed. The γ rays observed were $2_1^+ \rightarrow 0_1^+$, $4_1^+ \rightarrow 2_1^+$, and $(4)_2^+ \rightarrow 4_1^+$, the latter they describe as 'less expected'. Those results correspond to a relevant spectrum of ^{22}Mg being 0^+ (g.s.), 2_1^+ (1.247 MeV), 4_1^+ (3.308 MeV), $(4)_2^+$ (5.293 MeV), the ground state, first, second, and sixth excited states. Having not observed the relevant γ, they did not include the $2_2^+(4.402)$ state, the analogue of the 2_2^+ in ^{22}Ne, and which is known to decay via $M1 + E2$ to the 2_1^+ state. It also decays by undetermined γ decay to the ground state and to the 4_1^+ [24].

In ^{22}Ne, the equivalent tabulated $(4)_2^+$ state is at 5.523 MeV. This state is denoted uncertainly as $(4)^+$, with $J = 3$ also a possibility [24], though considering the spectrum of the mirror [4,24], the $J = 3$ possibility is less likely. It is the seventh excited state, with decays to lower states uncertain. (Ref. [24] gives only that the 4^+ J^π assignment comes from $L = 4$ in $(^6$Li$,d)$). It is shown as a dashed line in Fig. 1.

As it is unclear to what states this $(4)_2^+$ couples by γ emission, it is not possible to assign a β_L value as stringently as in Sec. IV A. Thus, the first calculation which includes the second 4^+ state assigns its β_2 to be that between states in the main rotational band, so the effect of its coupling is over- rather than underestimated. The second calculation assigns the same value as for the 2_2^+ state: 43% coupling strength of that between states in the principal rotor band. Fig. 1 graphically summarizes the states used in the various calculations presented.

Results of including this state in MCAS calculations are shown in Fig. 6, where, it is stressed, the parameters of the interaction potential are as listed in Table IV for all calculations. While the calculations including the $(4)_2^+$ do not change the ground state energy, indicating that within this model the ground state does not have any large component from mixing with this state, it does show a significant influence from the $(4)_2^+$ target state in the $\frac{7}{2}_1^+$ and $\frac{5}{2}_2^+$ compound states, as well as those of the speculated $\frac{9}{2}_1^+$ and $\frac{13}{2}_1^+$. A small change is also seen in the $\frac{3}{2}_1^+$. In the case where the coupling strength is 43% of that within the main rotor band, denoted (d), results are improved from the calculation (a) where the $(4)_2^+$ target state is not included, with the $\frac{7}{2}_1^+$ and $\frac{5}{2}_2^+$ being brought closer to observed energies.

The spectrum of ^{23}Ne from calculation (d) and experiment, within the energy range where this calculation is most pertinent, has been highlighted in a solid box. This is the best result. The result of (a) is highlighted with a dashed box.

B. Effects on the cross section

The MCAS results for the $n+^{22}$Ne cross section are shown in Fig. 7. It is important to note that these were not considered during the parameter fit, and as such the results are 'predictions' of the model.
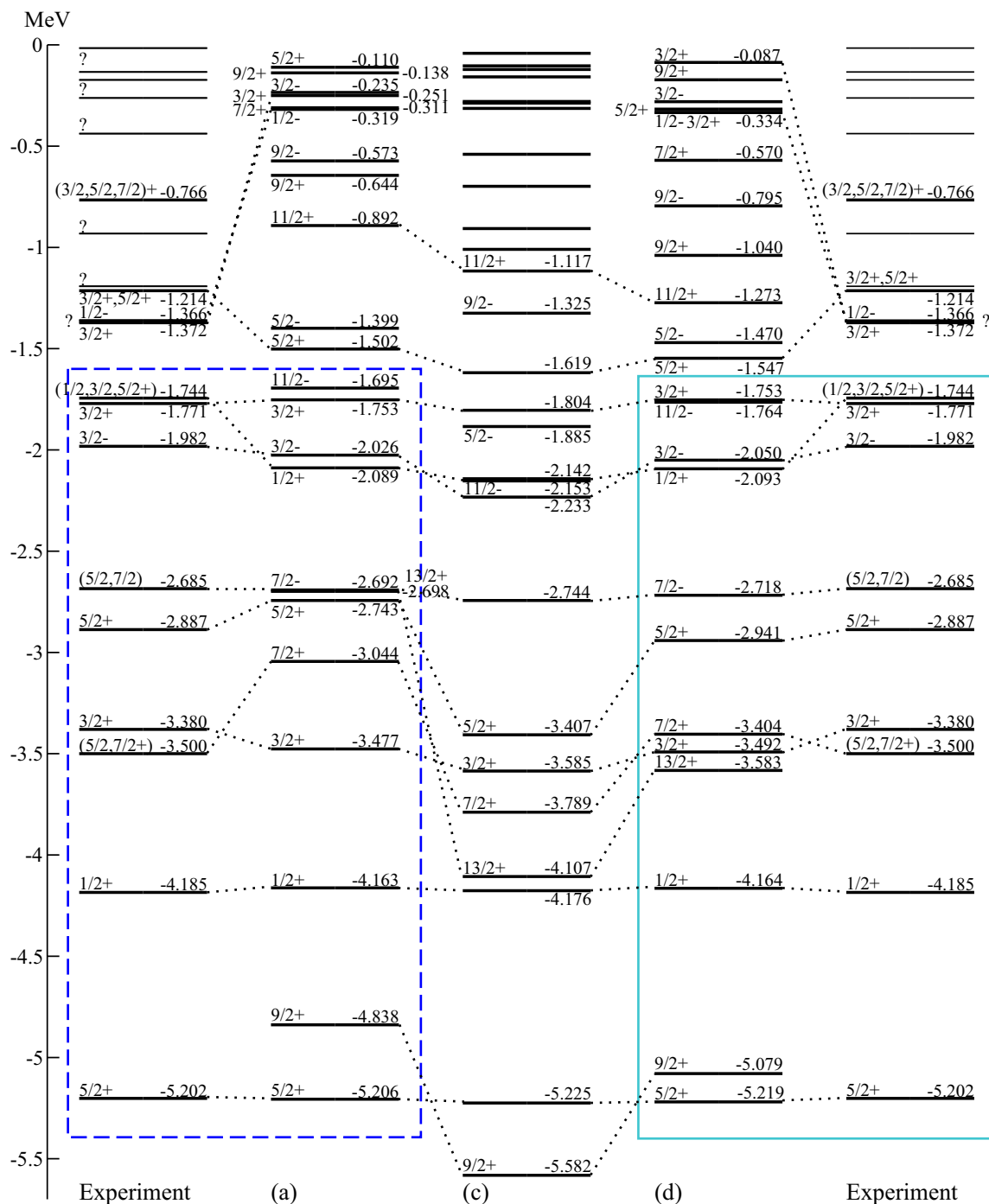
FIG. 6. (Color online) Experimental data compared to MCAS ^{23}Ne spectra using (a) 0_1^+, 2_1^+, 4_1^+, $\overline{2_2^+}$ (as per Fig. 2); (c) 0_1^+, 2_1^+, 4_1^+, $\overline{2_2^+}$, $(4)_2^+$ (as per Ref. [4]); and (d) 0_1^+, 2_1^+, 4_1^+, $\overline{2_2^+}$, $\overline{(4)_2^+}$. The bar denotes the use of reduced coupling for channels involving this state. Best result presented in the solid blue box.

Given the density of states around this threshold, and that the NA potential used has a limited energy range in which it well reproduces results, and that this was tuned to the deeply bound low-lying states, the study of an MCAS elastic cross section for neutron scattering can only be qualitative. As seen in Fig. 2, this span of energies is beyond where the current MCAS evaluations can accurately place centroids. While only

the elastic, and for incident energies above 1.274 MeV, the inelastic scattering processes are entertained with MCAS, the only missing possible reaction process in the energy range examined is that of neutron capture. However, capture cross sections for this system are negligible, with, for example, Ref. [36] giving the capture background below ∼0.5 MeV in the order of, at most, 100 μb. Thus, the sole factor in the
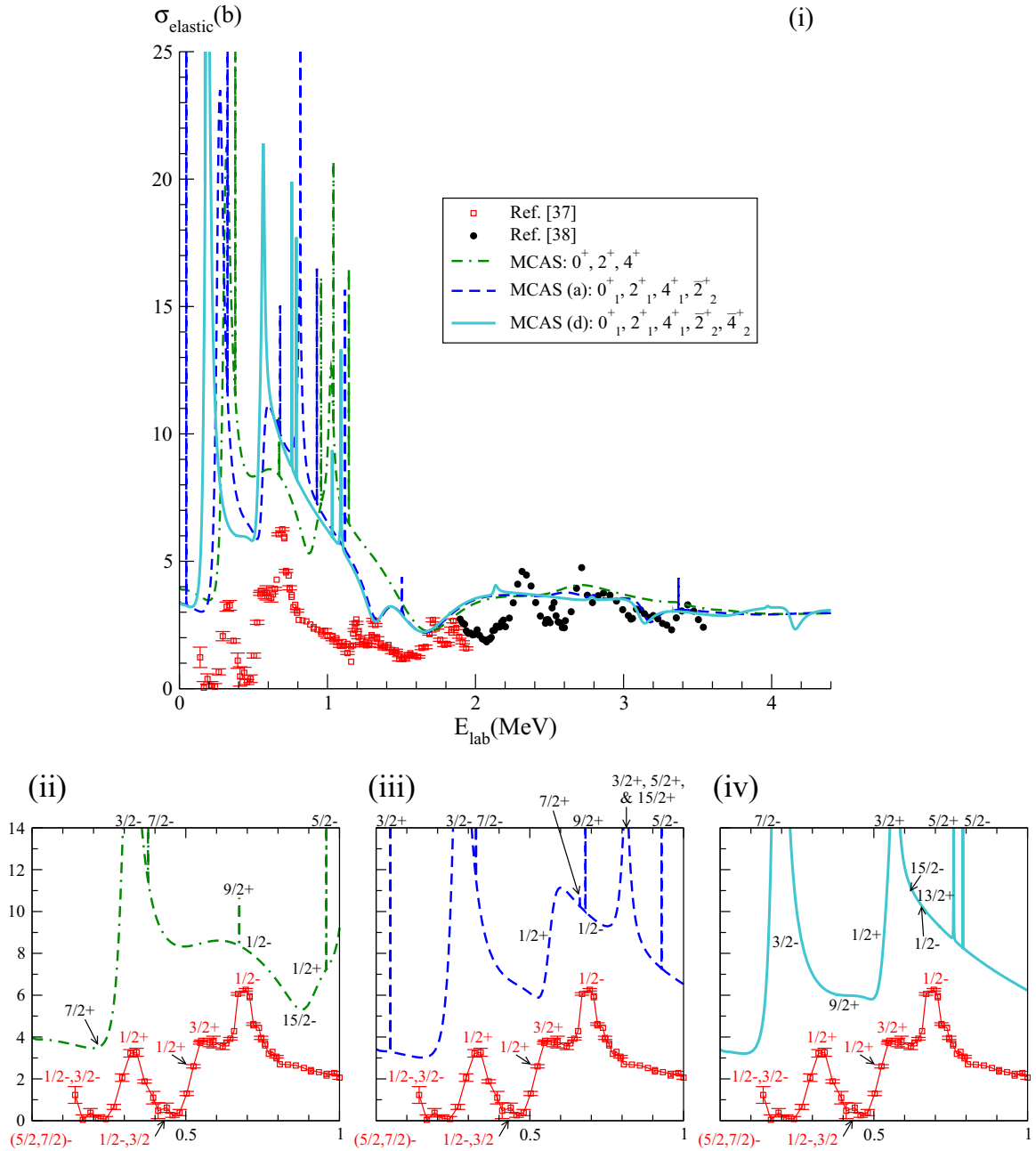
FIG. 7. (Color online) The MCAS $n+^{22}$Ne elastic cross section: (i) 0–4.4 MeV, three calculations; (ii) 0–1 MeV, 0_1^+, 2_1^+, 4_1^+ calculation; (iii) 0–1 MeV, 0_1^+, 2_1^+, 4_1^+, $\overline{2_2^+}$ calculation [corresponding to (a) in Figs. 2, 5, and 6]; and (iv) 0–1 MeV, 0_1^+, 2_1^+, 4_1^+, $\overline{2_2^+}$, $\overline{(4)_2^+}$ calculation [corresponding to (d) in Fig. 6]. (Red) squares from Ref. [37], black circles from Ref. [38], J^π assignments from Ref. [35].

overestimation of the elastic scattering cross section MCAS result at low energies is the limitation of the coupled-channel interaction used.

Despite the simplicity of the chosen interaction form, MCAS has been able to recreate some features of the observed data, which comes from Refs. [37] and [38] for 0.14 to 1.93 MeV and 1.89 to 3.54 MeV, respectively. This is shown in Fig. 7, where the marked experimental J^π assignments are from Ref. [35]. The result of the basic $0_1^+, 2_1^+, 4_1^+$ target state calculation is shown by the dotted-and-dashed line, the result

of calculation (a), with the addition of the $\overline{2_2^+}$ state (the bar denoting the weak coupling), is shown by the dashed line, and the result of (d), with the $\overline{(4)_2^+}$, is shown by the solid line. It should be noted that this is a region with a high density of observed states: as well as the seven marked J^π values, there are four further observed and two possibly observed resonances that have not been assigned J^π values between 0 and 0.6 MeV above threshold.

The upper panel shows that, above around 1.9 MeV, MCAS recreates the resonance background to a remarkably good

degree. It also shows that the addition of both the 2_2^+ and 4_2^+ states is required to begin some representation of the resonance structure seen at this energy.

In the lower panels, it is shown that the addition of the $\overline{2_2^+}$ changes the shape of the calculated cross section, and brings some resonance features into better agreement with experiment, principally the $\frac{1}{2}^+$ observed on the shoulder at 0.521 MeV (lab). In the three-state calculation we see this structure, but at 0.905 MeV (lab). Thus, the inclusion of weakly coupling target states is shown to have an impact over a wide range of energies.

The addition of the $\overline{(4)_2^+}$ state brings more features into agreement with data. In the four-state calculation, the $\frac{3}{2}^+$ resonance seen in the experimental data at 0.545 MeV (lab) is located at overly high energy, whereas in the five-state calculation the centroid is brought down to the appropriate energy. The addition of the $(4)_2^+$ brings the calculated $\frac{3}{2}^-$ closer to the uncertainly assigned $\frac{1}{2}^-, \frac{3}{2}^-$ resonance at 0.268 MeV (lab). Finally, in all three the cases, the $\frac{1}{2}^-$ resonance observed at 0.674 MeV (lab) is detected, though not discernible from the scattering background, and is placed correctly in energy.

VI. CONCLUSIONS

Historically, the multichannel algebraic scattering formalism when applied to a nucleon-nucleus system used a rotational collective model to describe the selected states of the nuclear target and of the interactions between those states and the extra nucleon. All coupling interactions were specified by single β_L deformation strengths. Most applications were of light mass systems and for a relative small range of neutron energies in which, usually, there were few target states deemed to belong to the main rotational band. Use of single values of β_L for the selected deformations, then sufficed to produce spectra of the compound system. For some systems of importance, however, it is necessary to include coupling to states outside of the main rotational band; such as cases where experiment shows γ decays from those extra states to ones within the collective band. Accordingly, MCAS has been extended to allow coupling of different strengths between some of the set of target states used.

This extended form of MCAS has been applied to the $n +$ ^{22}Ne system. The results showed that by varying the β_2 value of one state, the 2_2^+ (4.455 MeV), with regards to others has a marked effect upon the evaluated spectrum of the compound, ^{23}Ne. The value of coupling of the 2_2^+ state with the rotor band states ($0_1^+, 2_1^+$, and 4_1^+) was determined by using the $B(E2)$ values of the ground state γ decays of the 2_1^+ and 2_2^+ states. Treating the decays in a collective model defined the ratio of $\overline{\beta_2(2_2^+)}$ to that of $\beta_2(2_1^+)$. Addition of the $(4)_2^+$ state to the target set with coupling to others defined as being the same as the $\overline{\beta_2(2_2^+)}$, improves the description of the spectrum as well as the ^{22}Ne$(n,n)^{22}$Ne elastic cross section.

The MCAS cross section recreated some resonance features observed experimentally, and for higher energies reproduced the observed background. The importance of coupling to target states outside of the main rotor band was illustrated by the non-negligible changes they make to the cross section.

The system investigated in this work is highly complex, and there are avenues to improve the presented results in future studies. For example, the interpretation of the Pauli principle effect, by assuming only strictly forbidden or completely allowed shells could be relaxed. It is known in cluster physics that the allowance of intermediate 'Pauli hindrance' is important [3]. Such consideration may move unobserved low-lying high-spin states to higher energies, though we cannot exclude the possibility that a $\frac{9}{2}^+$ state may exist in the first few MeV of the spectrum.

APPENDIX

In this appendix, further details are presented of the NA scattering potential based on a Tamura [14] collective model with rotational character for even-mass targets.

Equation (11) presented the potential, in terms of its zeroth, first-, and second-order components of expansion in terms of the perturbation of the nuclear surface from spherical. It is in a form with all terms not dependent on L subsumed in equations $v^{(0)}(r)$, $v^{(1)}(r)$, and $v^{(2)}(r)$:

$$
\begin{aligned}
V_{cc'}(r) &= V_{cc'}^{(0)}(r) + V_{cc'}^{(1)}(r) + V_{cc'}^{(2)}(r) \\
&= \{v^{(0)}(r)\}_{cc'} \\
&\quad + \left\{ v^{(1)}(r) \sum_{L(\geqslant 2)} \beta_L \sqrt{\frac{4\pi}{2L+1}} \, [\mathbf{Y}_L \cdot \mathbf{Y}_L] \right\}_{cc'} \\
&\quad + \left\{ v^{(2)}(r) \sum_{L,L'(\geqslant 2)} \beta_L \beta_{L'} \sqrt{(2L+1)(2L'+1)} \right. \\
&\quad \left. \times \sum_{\ell} \frac{1}{2\ell+1} \, |\langle L0L'0|\ell 0\rangle|^2 \, [\mathbf{Y}_\ell \cdot \mathbf{Y}_\ell] \right\}_{cc'}.
\end{aligned}
$$

To determine the deformed channel potential, it is not simply a matter of taking the matrix elements of the radial operators between channels states c and c' and substituting them into Eq. (2). The channel potential expression involves matrix elements of the products of two operators and so one must first make symmetric the potential matrix form. With the zeroth order interaction, this is applicable only to the nondiagonal term involving the operator $I \cdot s$, so one replaces

$$
\begin{aligned}
V_{ss} w(r)[I \cdot s]|_{cc'} &\Rightarrow \tfrac{1}{2} V_{ss} \{w(r)[I \cdot s]\|_{c'c'} + [I \cdot s]|_{cc} w(r)\} \\
&\equiv \tfrac{1}{2}[V_{ss}^{(c)} + V_{ss}^{(c')}] w(r)[I \cdot s]|_{cc'}. \quad \text{(A1)}
\end{aligned}
$$

Thus, the zero-order term in Eq. (11) is

$$\{V^{(0)}(r)\}_{cc'} = \left\{\left[V_0^{(c)} + V_{ll}^{(c)}l(l+1)\right]w(r) + W_{ls}^{(c)}\frac{1}{r}\frac{\partial w(r)}{\partial r}\{\mathbf{l}\cdot\mathbf{s}\}\right\}\delta_{cc'} + \frac{1}{2}\left[V_{ss}^{(c)} + V_{ss}^{(c')}\right]\{\mathbf{I}\cdot\mathbf{s}\}_{cc'}\,w(r)\,. \tag{A2}$$

The $\delta_{cc'}$ is added to stress that the included terms contribute only on the diagonal. (This potential accounts for some of the discontinuities between the three- and four-state calculations in Figs. 3 and 4 when $s_2 = 0$. While the first term does not contribute, being diagonal in channels, the dependence of the second term on $\{\mathbf{I}\cdot\mathbf{s}\}_{cc'}$ has the consequence that, even with no deformation, channels of the same spin-parity I^π are coupled. Thus, the 2_2^+ state is linked to the 2_1^+.)

In the first- and second-order terms, the other two components also need be taken with symmetrised operators, and therefore

$$\{V^{(1)}(r)\}_{cc'} = -R_0\left\{\frac{\partial w(r)}{\partial r}\frac{1}{2}\left[V_0^{(c)} + V_0^{(c')} + V_{ll}^{(c)}\{\mathbf{l}\cdot\mathbf{l}\}_{cc} + V_{ll}^{(c')}\{\mathbf{l}\cdot\mathbf{l}\}_{c'c'}\right]\right.$$

$$- \frac{1}{2}R_0\frac{1}{r}\frac{\partial^2 w(r)}{\partial r^2}\left(W_{ls}^{(c)}\{\mathbf{l}\cdot\mathbf{s}\}_{cc} + W_{ls}^{(c')}\{\mathbf{l}\cdot\mathbf{s}\}_{c'c'}\right)\right\}\left[\sqrt{\frac{4\pi}{2L+1}}\beta_L\left[\mathbf{Y}_L\cdot\mathbf{Y}_L\right]\right]_{cc'}$$

$$- \frac{1}{2}R_0\frac{\partial w(r)}{\partial r}\sum_{c''}\left\{V_{ss}^{(c')}\left[\sqrt{\frac{4\pi}{2L+1}}\beta_L\left[\mathbf{Y}_L\cdot\mathbf{Y}_L\right]\right]_{cc''}\left[\mathbf{I}\cdot\mathbf{s}\right]_{c''c'} + V_{ss}^{(c)}\left[\mathbf{I}\cdot\mathbf{s}\right]_{cc''}\left[\sqrt{\frac{4\pi}{2L+1}}\beta_L\left[\mathbf{Y}_L\cdot\mathbf{Y}_L\right]\right]_{c''c'}\right\} \tag{A3}$$

and

$$\{V^{(2)}(r)\}_{cc'} = R_0^2\left\{\frac{1}{4}\frac{\partial^2 w(r)}{\partial r^2}\left[V_0^{(c)} + V_0^{(c')} + V_{ll}^{(c)}\{\mathbf{l}\cdot\mathbf{l}\}_{cc} + V_{ll}^{(c')}\{\mathbf{l}\cdot\mathbf{l}\}_{c'c'}\right]\right.$$

$$\left.+ \frac{R_0^2}{4}\frac{1}{r}\frac{\partial^3 w(r)}{\partial r^3}\left(W_{ls}^{(c)}\{\mathbf{l}\cdot\mathbf{s}\}_{cc} + W_{ls}^{(c')}\{\mathbf{l}\cdot\mathbf{s}\}_{c'c'}\right)\right\}$$

$$\times\left[\sum_{LL'}\beta_L\beta_{L'}\sqrt{(2L+1)(2L'+1)}\sum_{\ell\,\text{even}}^{2L}\frac{1}{(2\ell+1)}|\langle L0L'0|\ell0\rangle|^2\,[\mathbf{Y}_\ell\cdot\mathbf{Y}_\ell]\right]_{cc'}$$

$$+ \frac{R_0^2}{4}\frac{\partial^2 w(r)}{\partial r^2}\sum_{c''}\left\{V_{ss}^{(c)}\{\mathbf{I}\cdot\mathbf{s}\}_{cc''}\left[\sum_{LL'}\beta_L\beta_{L'}\sqrt{(2L+1)(2L'+1)}\sum_{\ell\,\text{even}}^{2L}\frac{1}{(2\ell+1)}|\langle L0L'0|\ell0\rangle|^2\,[\mathbf{Y}_\ell\cdot\mathbf{Y}_\ell]\right]_{c''c'}\right.$$

$$\left.+ V_{ss}^{(c')}\left[\sum_{LL'}\beta_L\beta_{L'}\sqrt{(2L+1)(2L'+1)}\sum_{\ell\,\text{even}}^{2L}\frac{1}{(2\ell+1)}|\langle L0L'0|\ell0\rangle|^2\,[\mathbf{Y}_\ell\cdot\mathbf{Y}_\ell]\right]_{cc''}\{\mathbf{I}\cdot\mathbf{s}\}_{c''c'}\right\}\,. \tag{A4}$$

The matrix elements of the operators $\mathbf{l}\cdot\mathbf{l}$, $\mathbf{I}\cdot\mathbf{s}$, and $\mathbf{l}\cdot\mathbf{s}$ are

$$\langle\mathbf{l}\cdot\mathbf{l}\rangle = \langle l'j'I'J|\mathbf{l}\cdot\mathbf{l}|ljIJ\rangle = \delta_{ll'}\delta_{jj'}\delta_{II'}l(l+1) \tag{A5}$$

and

$$\langle\mathbf{s}\cdot\mathbf{l}\rangle = \delta_{ll'}\delta_{jj'}\delta_{II'} \times \begin{cases} \frac{l}{2}, & \text{if} \quad j = l + \frac{1}{2} \\ -\frac{l+1}{2}, & \text{if} \quad j = l - \frac{1}{2} \end{cases}. \tag{A6}$$

The spin-spin matrix element is more complicated [17], namely,

$$\langle\mathbf{s}\cdot\mathbf{I}\rangle = (-)^{(j+j'+J)}\begin{Bmatrix} j' & j & 1 \\ I & I' & J \end{Bmatrix}\langle I'\|\mathbf{I}\|I\rangle\langle s\|\mathbf{s}\|s\rangle$$

$$= \delta_{II'}\delta_{ll'}(-)^{(1/2+j-j'+I+J+l)}\sqrt{(2j+1)(2j'+1)(2I+1)}\sqrt{\frac{3}{2}I(I+1)}\begin{Bmatrix} j' & j & 1 \\ I & I & J \end{Bmatrix}\begin{Bmatrix} \frac{1}{2} & l & j \\ j' & 1 & \frac{1}{2} \end{Bmatrix}. \tag{A7}$$

The operator is diagonal in I and l, and zero if either I or I' is zero.

Finally, the matrix elements of the scalar product of two rank L spherical harmonics are needed. They are

$$
\begin{aligned}
\langle \mathbf{Y}_L \cdot \mathbf{Y}_L \rangle &= \langle l'j'I'J | \mathbf{Y}_L(\hat{r}) \cdot \mathbf{Y}_L(\hat{\Upsilon}) | ljIJ \rangle \\
&= (-)^{(j+I'+J)} \begin{Bmatrix} j' & j & L \\ I & I' & J \end{Bmatrix} \left\langle \left(l'\tfrac{1}{2} \right) j' \| \mathbf{Y}_L(\hat{r}) \| \left(l\tfrac{1}{2} \right) j \right\rangle \langle I' \| \mathbf{Y}_L(\hat{\Upsilon}) \| I \rangle \\
&= (-)^{(j+I'+l'-\frac{1}{2})} \sqrt{(2j+1)(2j'+1)(2I+1)(2l+1)} \\
&\quad \times \frac{1}{4\pi}(2L+1)\langle I0L0|I'0\rangle\langle l0L0|l'0\rangle \begin{Bmatrix} j' & j & L \\ I & I' & J \end{Bmatrix} \begin{Bmatrix} l & \tfrac{1}{2} & j \\ j' & L & l' \end{Bmatrix},
\end{aligned} \tag{A8}
$$

which, on using the identity

$$
\begin{Bmatrix} l & \tfrac{1}{2} & j \\ j' & L & l' \end{Bmatrix} \langle l0L0|l'0\rangle = (-)^{(l+j'+\frac{1}{2})} \frac{1}{\sqrt{(2l+1)(2j'+1)}} \left\langle j\tfrac{1}{2}L0 \middle| j'\tfrac{1}{2} \right\rangle, \tag{A9}
$$

reduce to

$$
\begin{aligned}
\langle l'j'I'J | \mathbf{Y}_L(\hat{r}) \cdot \mathbf{Y}_L(\hat{\Upsilon}) | ljIJ \rangle &= (-)^{(J-\frac{1}{2}+I')} \frac{1}{4\pi} \sqrt{(2I+1)(2j+1)(2j'+1)(2L+1)} \\
&\quad \times \frac{1}{2}[1+(-)^{l+l'+L}]\langle I0L0|I'0\rangle \left\langle j-\tfrac{1}{2}j'\tfrac{1}{2} \middle| L0 \right\rangle \begin{Bmatrix} j' & j & L \\ I & I' & J \end{Bmatrix}.
\end{aligned} \tag{A10}
$$

---

[1] N. K. Timofeyuk, R. C. Johnson, and A. M. Mukhamedzhanov, Phys. Rev. Lett. **91**, 232501 (2003).

[2] N. K. Timofeyuk and P. Descouvemont, Phys. Rev. C **71**, 064305 (2005).

[3] C. Ritossa *et al.*, Astrophys. J. **515**, 381 (1999).

[4] A. Banu *et al.*, Phys. Rev. C **84**, 015803 (2011).

[5] T. Al-Abdullah *et al.*, Phys. Rev. C **81**, 035802 (2010).

[6] S. J. Jin *et al.*, Phys. Rev. C **88**, 035801 (2013).

[7] L. Canton and L. G. Levchuk, Nucl. Phys. A **808**, 192 (2008).

[8] C. Iliadis *et al.*, Astrophys. J. **142**, 105 (2002).

[9] F. Cavanna, R. Depalo, M.-L. Menzel, and LUNA Collaboration, AIP Conf. Proc. **1498**, 314 (2012).

[10] K. Amos, L. Canton, G. Pisent, J. P. Svenne, and D. van der Knijff, Nucl. Phys. A **728**, 65 (2003).

[11] L. Canton, G. Pisent, J. P. Svenne, D. van der Knijff, K. Amos, and S. Karataglidis, Phys. Rev. Lett. **94**, 122503 (2005).

[12] K. Amos *et al.*, Nucl. Phys. A **917**, 7 (2013).

[13] K. Amos, S. Karataglidis, D. van der Knijff, L. Canton, G. Pisent, and J. P. Svenne, Phys. Rev. C **72**, 064604 (2005).

[14] T. Tamura, Rev. Mod. Phys. **37**, 679 (1965).

[15] P. Fraser, K. Amos, L. Canton, G. Pisent, S. Karataglidis, J. P. Svenne, and D. van der Knijff, Phys. Rev. Lett. **101**, 242501 (2008).

[16] K. Amos *et al.*, Nucl. Phys. A **879**, 132 (2012).

[17] D. A. Varshalovich, A. N. Moskalev, and V. K. Kersonskii, *Quantum Theory of Angular Momentum* (World Scientific, Singapore, 1988).

[18] S. Karataglidis, P. Halse, and K. Amos, Phys. Rev. C **51**, 2494 (1995).

[19] S. Karataglidis, P. J. Dortmans, K. Amos, and R. deSwiniarski, Phys. Rev. C **53**, 838 (1996).

[20] S. Karataglidis and K. Amos, Phys. Rev. C **87**, 054623 (2013).

[21] OXBASH-MSU (the Oxford-Buenos-Aries-Michigan State University shell model code), A. Etchegoyen, W. D. M. Rae, and N. S. Godwin (MSU version by B. A. Brown, 1986); B. A. Brown, A. Etchegoyen, and W. D. M. Rae, MSUCL Report No. 524 (1986).

[22] E. K. Warburton and B. A. Brown, Phys. Rev. C **46**, 923 (1992).

[23] B. A. Brown and B. H. Wildenthal, Ann. Rev. Nucl. Part. Sci. **38**, 29 (1988).

[24] R. B. Firestone *et al.*, Nucl. Data Sheets **106**, 1 (2005).

[25] E. W. Schmid, in *Proceedings of the Workshop on Few-Body Problems in Nuclear Physics, Trieste, Italy, March 1978*, edited by G. Pisent, V. Vanzani, and L. Fonda (IAEA, Vienna, 1978), p. 389.

[26] E. W. Schmid, Z. Phys. A **297**, 105 (1980).

[27] R. A. Baldock, B. A. Robson, and R. F. Barrett, Nucl. Phys. A **351**, 157 (1981).

[28] E. W. Schmid and S. Saito, Z. Phys. A **306**, 37 (1982).

[29] K. Langanke and H. Friedrich, in *Advances in Nuclear Physics*, edited by J. W. Negele and Erich Vogt, Vol. 17 (Plenum, New York, 1986), pp. 223–363.

[30] G. Filippov and Y. Lashko, Phys. Rev. C **70**, 064001 (2004).

[31] Y. Lashko and G. Filippov, Phys. At. Nucl. **70**, 1017 (2007).

[32] R. de Swiniarski *et al.*, Phys. Rev. Lett. **28**, 1139 (1972).

[33] S. Raman, C. W. Nestor, Jr., and P. Tikkanen, At. Data Nucl. Data Tables **78**, 1 (2001).

[34] E. Sauvan *et al.*, Phys. Rev. C **69**, 044603 (2004).

[35] R. B. Firestone *et al.*, Nucl. Data Sheets **108**, 1 (2007).

[36] H. Beer *et al.*, Nucl. Phys. A **705**, 239 (2002).

[37] S. R. Salisbury, R. A. Chalmers, D. B. Fossan, and F. J. Vaughn, Bull. Am. Phys. Soc. **11**, 28 (1966), Data available at https://www-nds.iaea.org/x4toc4-master/dev/ver1/exfor/113/11340.x4.

[38] S. Sikkema, P. J. Pasma, and H. H. V. Barneveld, Nucl. Phys. **5**, 351 (1958).